

UNCERTAINTY-DRIVEN ENSEMBLES OF DEEP ARCHITECTURES FOR MULTICLASS CLASSIFICATION. APPLICATION TO COVID-19 DIAGNOSIS IN CHEST X-RAY IMAGES

Juan E. Arco^{1,*}, Andrés Ortiz², Javier Ramírez¹, Francisco J. Martínez-Murcia²,
Yu-Dong Zhang³, Juan M. Górriz¹

¹ Department of Signal Theory, Networking and Communications, Universidad de Granada

² Department of Signal Theory, Networking and Communications, Universidad de Malaga

³ School of Informatics, University of Leicester, Leicester, LE1 7RH, Leicestershire, UK

ABSTRACT

Respiratory diseases kill million of people each year. Diagnosis of these pathologies is a manual, time-consuming process that has inter and intra-observer variability, delaying diagnosis and treatment. The recent COVID-19 pandemic has demonstrated the need of developing systems to automatize the diagnosis of pneumonia, whilst Convolutional Neural Network (CNNs) have proved to be an excellent option for the automatic classification of medical images. However, given the need of providing a confidence classification in this context it is crucial to quantify the reliability of the model's predictions. In this work, we propose a multi-level ensemble classification system based on a Bayesian Deep Learning approach in order to maximize performance while quantifying the uncertainty of each classification decision. This tool combines the information extracted from different architectures by weighting their results according to the uncertainty of their predictions. Performance of the Bayesian network is evaluated in a real scenario where simultaneously differentiating between four different pathologies: control vs bacterial pneumonia vs viral pneumonia vs COVID-19 pneumonia. A three-level decision tree is employed to divide the 4-class classification into three binary classifications, yielding an accuracy of 98.06% and overcoming the results obtained by recent literature. The reduced preprocessing needed for obtaining this high performance, in addition to the information provided about the reliability of the predictions evidence the applicability of the system to be used as an aid for clinicians.

Index Terms— Pneumonia; COVID-19; Bayesian Deep Learning; Uncertainty; Ensemble classification.

1. INTRODUCTION

Respiratory illness is the most common cause of death and disability in the world. According to the World Health Organization (WHO), tuberculosis kills 1.4 million people each year, whereas pneumonia is a leading cause of death among children under 5 years old (World Health Organization, 2017). Although the rate of pneumonia is decreasing worldwide (World

Health Organization, 2016), an annual fatality rate of approximately 4 million is still observed. This disease is a form of acute respiratory infection that affects lungs, and based on the infectious pathogen, it can be bacterial, viral and fungal (Gilani et al., 2012). Doctors can identify the presence of pneumonia from a wide range of medical imaging such as computed tomography (CT) (Feng et al., 2015), chest X-ray (CXR) (Kunz et al., 2018) or magnetic resonance imaging (MRI) (Syrjala et al., 2017). The quality improvement in X-ray imaging and its low cost has popularized the use of CXR as a diagnostic tool for pneumonia. However, this is not a straightforward task and success in pneumonia detection depends on many factors. One of the most important ones is that diagnosis is still largely dependent on the expertise of the radiologist (Chandra et al., 2020). The pathology associated with pneumonia is often overlapping with other abnormal conditions of the lungs. Besides, the complex and vague anatomical structures in the lung fields can also affect the expert's opinion (Maduskar et al., 2015). This leads to a manual, time-consuming process that has inter and intra-observer variability, which may delay diagnosis and treatment. The use of image processing methods along with machine learning algorithms directed to find disease-related patterns play a decisive role in the improvement of the diagnosis accuracy.

Previous works have employed machine learning (ML) algorithms for the automatic detection of a wide range of pathologies such as Parkinson's or Alzheimer's disease (Castillo-Barnes et al., 2018; Górriz et al., 2020; Zhang et al., 2020b), and most recently, pneumonia (Chandra et al., 2020; Elaziz et al., 2020; Wang et al., 2021a; Zhang et al., 2020). In this direction, CAD (computer-aided diagnosis) systems can be an excellent tool for overcoming the weakness of current procedures for detecting pneumonia. In fact, they can assist radiologists by reducing their workload, serving as an B-reader in diagnosis and reducing the variability across doctors. Classification systems employed in CAD tools have the following general structure: i) delimitation of the regions of interest (ROI) to focus the analysis on them, ii) features extraction from these regions, iii) classification based on those features (Jaeger et al., 2014; Liu and Pang, 2020; Xu et al., 2006). Since pneu-

* Corresponding author: jearco@ugr.es

monia affects lungs, it seems obvious that the ROI must delimit the shape and boundaries of lungs (Hogeweg et al., 2015; Van Ginneken et al., 2001). Several studies have provided different methods for lung segmentation (Ahmad et al., 2015; Candemir et al., 2014; Guan and Huang, 2020; Hassen et al., 2013; J et al., 2017; Vajda et al., 2018; Yang et al., 2018). Ahmad et al. (2015) proposed an unsupervised approach based on Gaussian derivatives filters and Fuzzy C-Means clustering. This method demonstrated not only good performance measures (accuracy of 0.9) but also robustness and speed. Regardless how features are computed they are then classified using a specific algorithm. Previous studies have successfully employed a wide range of classifiers for the detection of pulmonary diseases, such as DT (Decision Tree, Porcel et al., 2008; Zhang et al., 2020a), NB (Naïve Bayes, Chapman et al., 2011; Ma et al., 2015), or KNN (k -Nearest Neighbors (KNN), Ajin and Mredhula, 2017; Chen et al., 2015). However, literature has shown that Support Vector Machine (SVM) (Gu et al., 2018; Yahyaoui and Yumusak, 2018) usually outperforms the other algorithms (Chandra et al., 2020; Uppaluri et al., 1999).

Unlike classical methods based on the extraction of pre-defined features, deep neural networks build a specific feature space for the optimal class separation by means of a learning process. The emergence of these approaches has revolutionized the automatic classification of medical images. Recently, a number of studies have demonstrated the high flexibility and performance that this approach provides (Kermany et al., 2018; Mittal et al., 2020; Varshni et al., 2019; Wang et al., 2017). Rajpurkar et al. (2017) proposed a 121-layer convolutional neural network (CNN) to identify pneumonia and localize the most indicative areas of this pathology. The algorithm provided a relatively low accuracy (76.8%), but it was able to distinguish between 14 different pathologies. Other works have utilized transfer learning on the ImageNet dataset, yielding an accuracy of 82%, 87% and 92% for Xception, VGG16 and VGG19 models, respectively (Abiyev and Ma'aitah, 2018). It is clear that deep learning models can effectively identify the presence of a certain pathology. However, there are some scenarios where they take a decision (i.e. if a patient suffers from pneumonia or not) even though they do not know the answer since the classification outcome only relies on the most activated neuron of the output layer. Kendall and Gal (2017) demonstrated the need of evaluating the uncertainty of a model's predictions in order to improve the decisions of the system. Bayesian deep learning models offer a practical solution for understanding the uncertainty of the decisions of a deep learning model (Gal, 2016). Specifically, they model a combination of aleatoric and epistemic uncertainty in order to increase loss robustness to noisy data, which usually leads to a boost in performance (Kendall and Gal, 2017). Most importantly, the additional information related to the reliability of the classification results makes this alternative quite interesting for being used in situations where the consequences of an error could be critical.

The recent COVID-19 pandemic has demonstrated the need of developing systems to automatize the diagnosis of pneumonia. It seems clear that a wrong diagnosis can have a dramatic effect in patient's health. In this work, we employ an ensemble classification system based on a Bayesian Deep Learning approach in order to maximize performance while quantifying the uncertainty of each classification decision. In particular, we combine seven CNN with the same structure, but differing in the kernel sizes of their convolutional layers. This allows the classification system to extract relevant features of different size and shape. The global classification is performed by combining the predictions of the different classifiers. The contribution of each individual classifier depends on the uncertainty of their predictions: the lower the uncertainty, the higher the weight, and vice versa. Performance of the Bayesian network is evaluated in a range of real scenarios of incremental difficulty: from the simplest one where trying to distinguish between control vs pneumonia patients to a multiclass context where simultaneously differentiating between four different pathologies: control vs bacterial pneumonia vs viral pneumonia vs COVID-19 pneumonia. The main contributions of our work can be summarized as follows:

- A novel and accurate tool for the automatic diagnosis of pneumonia, in addition to the identification of the cause of the pathology (bacteria, virus, COVID-19).
- The Bayesian nature of the Residual Network proposed in this work quantifies the reliability of the classification predictions.
- The combination of networks with different kernel sizes allows the identification of pneumonia patterns regardless of their shape and extension.
- Our approach employs the uncertainty of the predictions of each individual classifier to weigh their contribution to the ensemble global decision.

2. MATERIAL

2.1. Dataset

We have used the dataset available in Kaggle (2020b) for controls and patients who suffered from a bacterial or a non-COVID19 pneumonia. According to the information described in Kermany et al. (2018), the CXR images were selected from retrospective cohorts of pediatric patients of one to five years old from Guangzhou Women and Children's Medical Center, Guangzhou. All CXR images were obtained as part of patient's routines clinical care. Institutional Review Board (IRB)/Ethics Committee approvals were obtained. The work was conducted in a manner compliant with the United States Health Insurance Portability and Accountability Act (HIPAA)

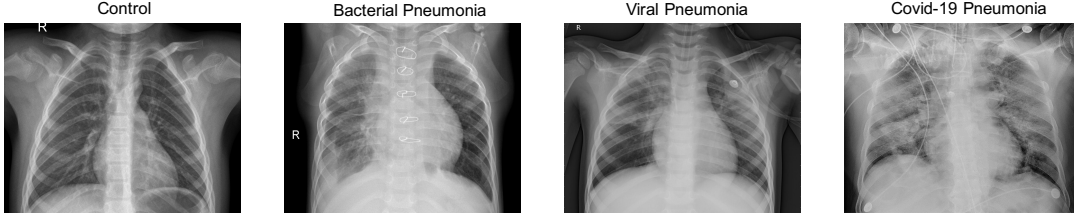


Fig. 1. From left to right, CXR image of a control, bacterial pneumonia, viral pneumonia and COVID-19 pneumonia. Note some clear artifacts in COVID-19 image.

and was adherent to the tenets of the Declaration of Helsinki. Kermany et al. (2018) collected and labeled a total of 6374 CXR images from children, including 4273 characterized as depicting pneumonia and 1583 normal. From those patients diagnosed with pneumonia, 2786 were labeled as bacterial pneumonia, whereas 1487 were labeled as viral pneumonia. The dataset containing COVID-19 patients is available in Kaggle (2020a) and includes 576 CXR images from adults. Figure 1 shows the CXR image from a control (CTL), and a patient suffering from a bacterial (BAC), a viral (VIR) and a COVID19 (CVD19) pneumonia.

2.2. Image preprocessing

When working with medical images, it is crucial to apply a preprocessing that improves the subsequent classification performance. This is especially important in CXR images, where low X-ray radiation and movement during image acquisition result in noisy and low-resolution images. However, this preprocessing must adapt images to the needs of the neural network. Due to computational and memory requirements, we downsampled the input images to obtain a final map of size 224×224 . We also performed an intensity normalization procedure for each individual image based on standardization. Each image was transformed such the resulting distribution has a mean (μ) of 0 and a standard deviation (σ) of 1, as follows:

$$I' = \frac{I - \mu}{\sigma} \quad (1)$$

where I is the original image and I' is the resulting one.

3. METHODS

3.1. Deep learning

The use of algorithms based on deep learning has revolutionized the analysis of medical images (Krizhevsky et al., 2012; Martínez-Murcia et al., 2018; Ortiz et al., 2016; Segovia et al., 2016). From the ImageNet classification benchmark (Schmidhuber, 2015), CNNs have been used more than any other pattern recognition algorithm in medical image classification.

This architecture emerged as an attempt of replicating the behavior of neurons. Briefly, CNNs combine different steps based on convolution and pooling to allow the identification of different patterns and low and high-level features (Martínez-Murcia et al., 2018; Payan and Montana, 2015). The main component of a CNN is known as convolutional layer. This operator takes the tensor \mathbf{V}_{i-1} containing the activation map of the previous layer $i - 1$. Thus, the target layer (i) learns a set of N filters \mathbf{W}_i with a bias term \mathbf{b}_i , as follows:

$$\mathbf{V}_i = f_a(\mathbf{W}_i * \mathbf{V}_{i-1} + \mathbf{b}_i) \quad (2)$$

where $f_a(*)$ is the activation function (Martínez-Murcia et al., 2018). For a three-dimensional environment (\mathbf{V}_{i-1}) of size $H \times W \times D \times C$ (height, width, depth and number of channels, respectively), \mathbf{W}_i is of size $P \times Q \times R \times S \times K$ where K is the number of filters. The k th convolution term for the k th filter is

$$\mathbf{W}_{ik} * \mathbf{V}_{i-1} = \sum_{u=0}^{P-1} \sum_{v=0}^{Q-1} \sum_{w=0}^{R-1} [\mathbf{W}_{ik}(P-u, Q-v, R-w) \mathbf{V}_{i-1}(x+u, y+v, z+w)] \quad (3)$$

Once convolution is performed, the activation of the filters in layer i are stored and passed to the next layer $i + 1$. It is of great importance to set properly the values for all the hyperparameters, striking a balance between performance and model complexity. One of these parameters is the number of filters: the higher this number is, the more patterns the model is able to learn. There is no consensus in literature about the ideal number of filters, probably because different problems need CNNs with different configurations, but numbers that are a power of 2 are usually taken.

3.2. Bayesian Deep learning

Despite the high performance that Deep Learning models have demonstrated, recent works have claimed the need of computing the uncertainty of a model, a measure that allows to identify situations where the classifier does not know the answer. To do so, it would be necessary to estimate the level of

uncertainty of a prediction in order to reject it in case its value was too high. Bayesian deep learning offers a framework for understanding uncertainty with deep learning models (Wang and Yeung, 2016). There are two main types of uncertainty that can be estimated in Bayesian modeling: epistemic and aleatoric (Gal, 2016; Kiureghian and Ditlevsen, 2009). Epistemic uncertainty is inherent to the model, which means that it can be reduced by increasing the data processed by the model. Estimating the epistemic uncertainty requires to model distributions over the different parameters of the model. This allows to optimize the network according to the average of all possible weights.

Let \mathbf{x} be a feature vector and \mathbf{W} the weights of a Bayesian Neural Network (BNN). Considering the output of the network as $\mathbf{f}^{\mathbf{W}}(\mathbf{x})$, the model likelihood can be defined as $p(\mathbf{y}|\mathbf{f}^{\mathbf{W}}(\mathbf{x}))$. For a given dataset $\mathbf{X} = \{\mathbf{x}_1, \dots, \mathbf{x}_N\}$, $\mathbf{Y} = \{\mathbf{y}_1, \dots, \mathbf{y}_N\}$, the Bayesian inference computes the posterior probability over the weights $p(\mathbf{W}|\mathbf{X}, \mathbf{Y})$.

Cipolla et al. (2018) demonstrated that applying dropout before every weight layer in a neural network is mathematically equivalent to an approximation to the probabilistic deep Gaussian process (Damianou and Lawrence, 2013). Briefly, they showed that the dropout objective minimizes the Kullback-Leibler divergence between an approximate distribution and the posterior one of a deep Gaussian process. A popular technique relies on the use of Monte Carlo dropout sampling to place a Bernoulli distribution over the network’s weights. Dropout is widely used as a regularization procedure during training (Srivastava et al., 2014). However, when applied during the testing phase, this method allows to obtain a distribution for the output predictions (Jospin et al., 2020; Li and Gal, 2017). The statistics of this distribution reflect the model’s epistemic uncertainty.

Aleatoric uncertainty is usually referred as the uncertainty inherent to the data, and can be divided into two sub-categories: i) homoscedastic uncertainty, which remains stable for every input of the model; and ii) heteroscedastic, which assumes that noise varies for the different inputs of the model (Le et al., 2005; Nix and Weigend, 1994). Heteroscedastic uncertainty can be modeled by modifying the loss function used by the neural network. Since this uncertainty is a function of the input data, employing a deterministic mapping from inputs to model outputs can allow the estimation of the uncertainty. For a typical Euclidean loss $L = \|y - \hat{y}\|^2$, the Bayesian version will be given by $L = \frac{\|y - \hat{y}\|^2}{2\sigma^2} + \frac{1}{2} \log \sigma^2$. In the latter one, the model predicts both \hat{y} and variance σ^2 , so that if model prediction is not good, the residual term will be attenuated by increasing σ^2 . Therefore, the term $\log \sigma^2$ prevents uncertainty growing until infinite, leading to a learned loss attenuation. The process for homoscedastic uncertainty is essentially the same, but considering the uncertainty like a free parameter instead of a model output.

In this work, we have employed a Bayesian version of the ResNet-18 CNN (He et al., 2016). The output layer con-

tained 2 neurons with softmax activation. Besides, dropout was used to prevent overfitting, and Batch Normalization for convergence. The Bayesian nature of this net is obtained by replacing the deterministic weights along the network by a distribution over these parameters. This means that instead of optimising the network weights, an average of all possible weights was computed. As a result, the loss function depends on two factors: the softmax values (as in the non-Bayesian modality) and the Bayesian categorical cross entropy, which is based on the input variance (see Kendall and Gal (2017) for more details). Figure 2 summarizes the architecture of the Bayesian network.

3.3. Multi-level Ensemble Classification

Patterns associated with each type of pneumonia are similar among different subjects. However, there are some factors like the virulence of the disease and the presence of other pulmonary findings that can affect the identification of the patterns associated with the different pathologies. One crucial aspect is to select an optimal kernel size for the convolutional operators of the neural network that can properly extract the relevant information. Moreover, this is even more important when images used to train the network come from different sources, and when they can have different sizes and aleatory artifacts. To overcome this issue, we employed seven neural networks, each one of them with a different kernel size value in the range [3 – 15] with increments of two. This means that the kernel size assigned to the first network was 3, 5 for the second network and so on, until a size of 15 for the seventh CNN. The number of neural networks and their kernel sizes were selected in order to strike a balance between performance and computational cost. Finally, each individual classifier was then combined into a global one following an ensemble classification procedure.

Previous studies have employed majority voting to fuse the output of the base classifiers (Chandra et al., 2021; Zhou et al., 2020). Given the Bayesian nature of the networks employed in this work, we computed the weights of each classifier as a function of the uncertainty given by each one of them for each test image (see Figure 3). If the uncertainty of a classifier in a specific prediction was high, it would have a low contribution to the final ensemble, and vice versa (Liu et al., 2012). Defining $u_l^k(\mathbf{y})$ as the uncertainty of the test sample \mathbf{y} obtained from the k -th classifier corresponding to the l -th class, the empirical average of the l -th weights (inverse of uncertainties) over the K classifiers can be calculated as follows:

$$E_l(\mathbf{y}) = \frac{\sum_{k=1}^K \frac{1}{u_l^k(\mathbf{y})}}{K} \quad (4)$$

The class label of the test sample \mathbf{y} is then assigned to the class with the maximum average weight as:

$$Label(\mathbf{y}) = \arg \max_l E_l(\mathbf{y}) \quad (5)$$

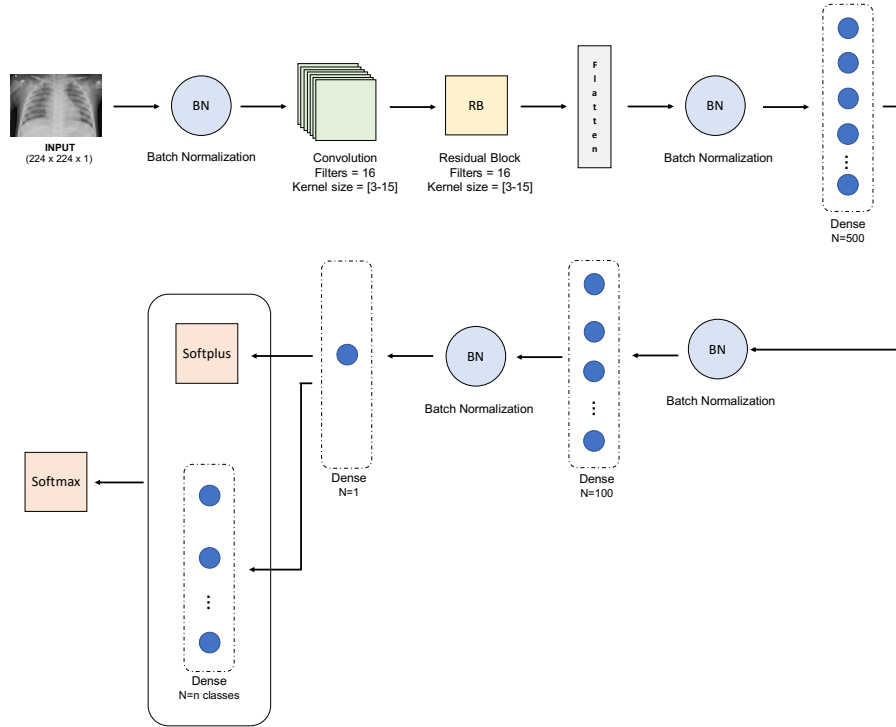


Fig. 2. Diagram of the Bayesian framework of each individual network within the ensemble.

Detecting the presence of pneumonia when comparing to healthy subjects is an interesting initial step in the development of a CAD system. However, it is much more useful to identify exactly the type of pneumonia patients suffer from. As described in Section 2.1, the database used in this work contains CXR images of healthy subjects (controls) and images from three types of pneumonia: bacterial, viral and COVID-19. In order to perform the multiclass classification, we employed a decision tree based on the One-versus-all (OVA) approach (Galar et al., 2011; Gao et al., 2021; Zhou and Fujita, 2017). This alternative divides a multiclass problem into a number of binary sub-problems. In each one of them, one of the classes is considered as the positive class, whereas the other classes are the negative class. Following this framework, we used a decision tree with three levels in order to distinguish between the different pathologies. In each level, an ensemble of different kernel sizes was employed. This led to a two-level ensemble classification: one ensemble for the combination of different kernels, and another one for combining binary classifiers to perform multiclass classification. The decision tree relies on a process that can be summarized as follows:

- First level: classification between normal *vs* pneumonia. The second class contains subjects diagnosed from the three different types of pneumonia (bacterial, viral, and COVID-19).

- Second level: classification between bacterial *vs* viral pneumonia. The second class corresponds to images from subjects with pneumonia due to different viruses (no-COVID-19 or COVID-19).
- Third level: classification between no-COVID-19 *vs* COVID-19.

Figure 4 depicts a visual representation of how the decision tree works. Images that are labelled as pneumonia in the first level are passed to the second one. Similarly, images labelled as viral pneumonia continue to the third level in order to identify whether the virus that produced the pneumonia was COVID-19 or not. It is worth mentioning that the binary classifier employed in each level has the same ensemble structure that the one explained in Section 3.3.

3.4. Performance evaluation

For all experiments, a 5-fold stratified cross-validation scheme was used to estimate the generalization ability of our method (Kohavi, 1995). The performance of the classification frameworks was evaluated in terms of different parameters from the confusion matrix, which can be computed as follows:

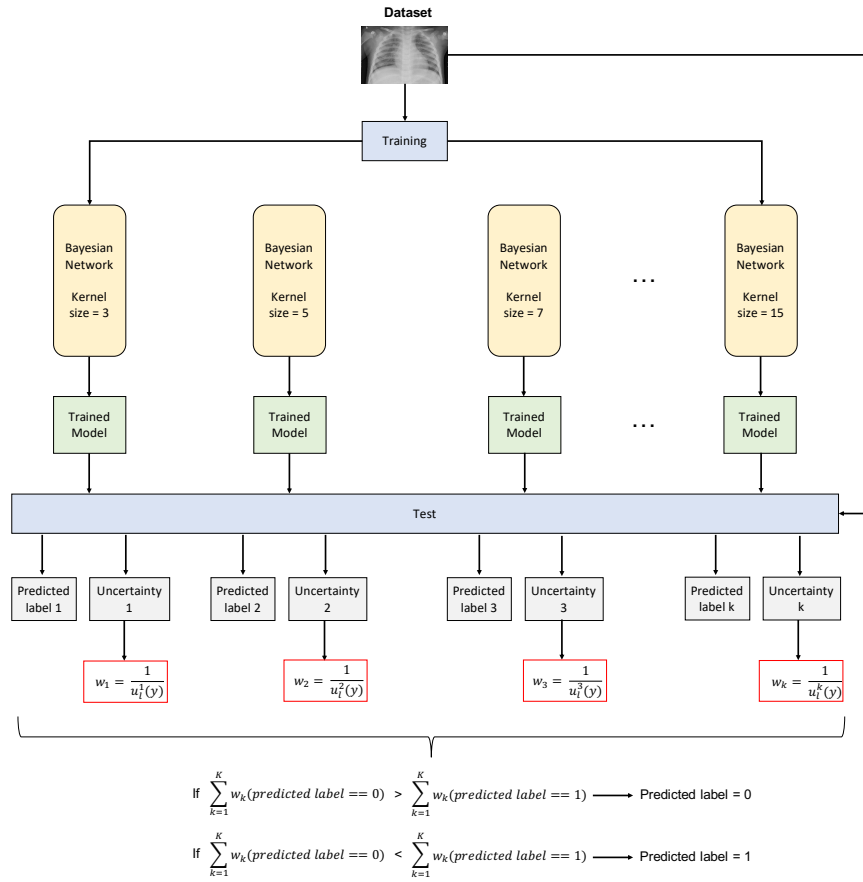


Fig. 3. Schema of the ensemble architecture proposed in this work based on the uncertainty in the prediction of each individual classifier.

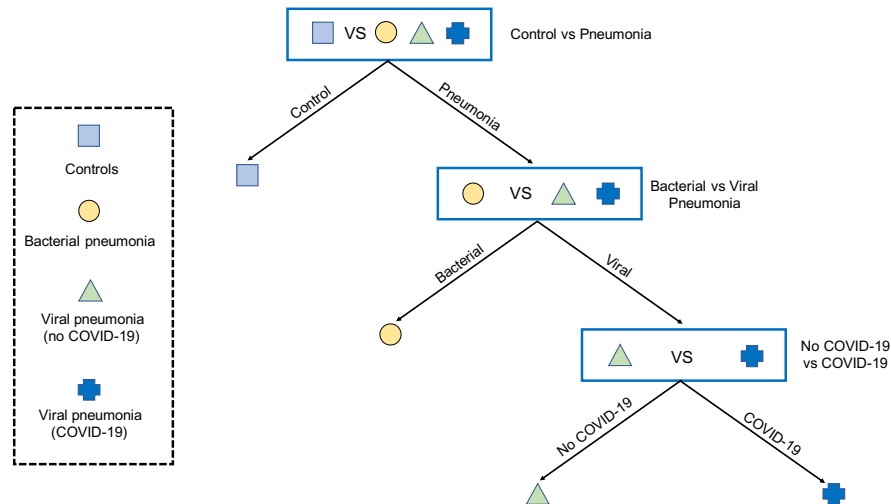


Fig. 4. Schematic representation of the decision tree employed for the multiclass classification.

$$\begin{aligned}
Acc &= \frac{T_P + T_N}{T_P + T_N + F_P + F_N} & Sens &= \frac{T_P}{T_P + F_N} \\
Spec &= \frac{T_N}{T_N + F_P} & AUC &= \frac{1}{2} \left(\frac{T_P}{P} + \frac{T_N}{N} \right) \\
Prec &= \frac{T_P}{T_P + F_P} & F1 - score &= \frac{2 \times Prec \times Sens}{Prec + Sens}
\end{aligned} \tag{6}$$

where T_P is the number of pneumonia patients correctly classified (true positives), T_N is the number of control patients correctly classified (true negatives), F_P is the number of control subjects classified as pneumonia (false positives) and F_N is the number of pneumonia patients classified as controls (false negatives). We also employed the area under the curve ROC (AUC) as an additional measure of the classification performance (Hajian-Tilaki, 2013; Mandrekar, 2010). Since classes were unbalanced (e.g. the number of pneumonia patients was higher than controls), we incorporated the weights of the classes into the cost function in order to the majority class does not contribute more than the minority one.

Given the ensemble nature of the system proposed in this work, we employed a kappa-uncertainty diagram to evaluate the level of agreement of the different classifier outputs while correcting for chance (Rodriguez et al., 2006; Wang et al., 2019). This measure is based on Cohen’s kappa coefficient (Cohen, 1960), which is widely accepted as the de facto standard for measurement of interannotator agreement (Di Eugenio and Glass, 2004). Specifically, the kappa statistic compares an observed accuracy with an accuracy obtained by chance, providing a measure of how closely instances classified by a classifier match the ground truth. Mathematically, Cohen’s kappa can be defined as:

$$k = \frac{p_A - p_E}{1 - p_E} \tag{7}$$

where p_A is the observed relative agreement between two annotators, and p_E is the probability of agreement by chance. Although acceptable kappa statistic values vary on the context, the closer to 1, the better the classification. Section 5 summarizes the kappa scores obtained by different members of the ensemble classifier, as well as revealing the relationship between the uncertainty of Bayesian networks and kappa values.

As explained in Section 3.3, a decision tree was employed for multiclass classification. In order to build the kappa-uncertainty diagram explained above, a combination of the uncertainties of the different levels of the tree has to be computed. To do so, we employed a method known as summation in quadrature (White, 2008), described as follows:

$$u_c(y) = \sqrt{\sum_{i=1}^n [c_i u(x_i)]^2} \tag{8}$$

where $u_c(y)$ is the combined uncertainty, c_i is the sensitivity coefficient and $u(x_i)$ is the standard uncertainty.

4. EVALUATION

4.1. Experimental setup

In this work we propose a method to extract the relevant information from CXR images that allows the identification of pneumonia. To do so, we define two experiments:

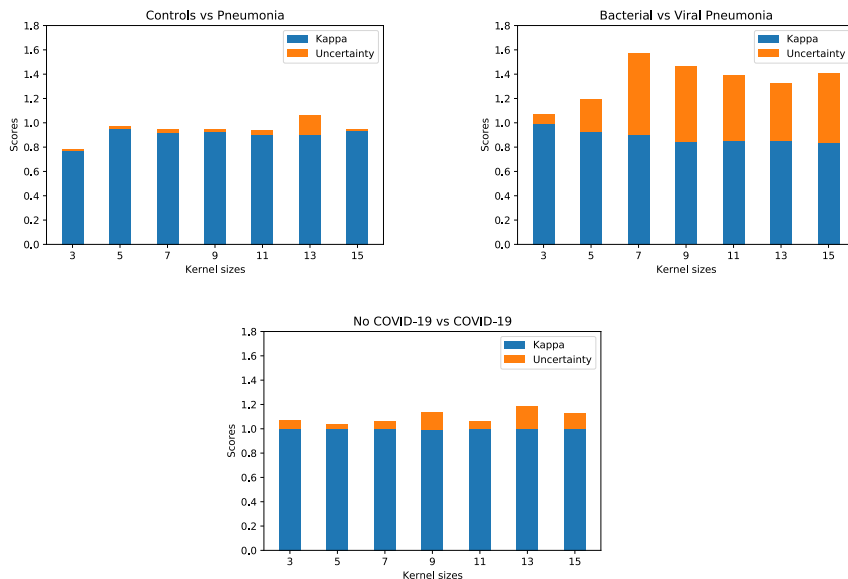
- **Experiment 1: Binary Classification** between different groups under three scenarios: **CTL vs PNEU**, which includes all images labelled as CTL and PNEU; **BAC vs VIR**, which divides the images from people diagnosed from pneumonia regarding the cause of the disease is a bacteria or a virus; **NO-COVID-19 vs COVID-19** for viral pneumonia. The aim is to identify whether the virus that produced pneumonia was COVID-19 or not. The whole Bayesian CNN was trained using the Adam optimization algorithm (Kingma and Ba, 2017), with learning rate 0.001, $\phi = 0.9$ and a decay of 0.001). The number of epochs employed for training the system was 15, 20 and 25, for the CTL vs PNEU, BAC vs VIR and NO-COVID-19 vs COVID-19 scenarios, respectively. We used the Keras library over Tensorflow with some custom modules.
- **Experiment 2: Multiclass Classification** by using a decision tree in order to distinguish between the four different pathologies contained in the database. A binary classification is employed in each of the three levels of the tree. The first level corresponds to the CTL vs PNEU classification, the second one contains the BAC vs VIR comparison, whereas in the third level, the distinction between NO-COVID-19 vs COVID-19 is performed. These binary classifiers employ the same framework and configuration as in Experiment 1.

5. RESULTS

We first explore how performance varies for the different kernel sizes of the individual classifiers for all the binary classifications performed (see Figure 5). We can see that kappa score slightly varies when increasing the kernel size in the three classification contexts. With reference to uncertainty, only in the BAC vs VIR scenario uncertainty values drastically change for different kernel sizes. Therefore, there is not a tendency that let us assure that there is a relationship between these two variables. It is important to note the high levels of uncertainty in this classification context when comparing to the first and the third one, which manifests the extreme difficulty of this specific classification. It is not surprising that differentiating between a control and a patient who suffer from pneumonia is a considerably easier task. However, these findings point out that there is a larger difference in the spatial patterns associated with COVID-19 vs no-COVID-19 than in

Table 1. Performance of the ensemble classification approach proposed in this work in the different contexts evaluated.

Experiment	Acc (%)	Sens (%)	Spec (%)	Prec (%)	AUC (%)	F1-score (%)
CTRL vs PNEU	97.27 \pm 3.37	96.41 \pm 4.47	99.94 \pm 0.13	99.98 \pm 0.04	98.17 \pm 2.22	98.11 \pm 2.38
BAC vs VIR	98.43 \pm 0.95	98.16 \pm 1.17	98.79 \pm 0.73	99.09 \pm 0.56	98.48 \pm 0.92	98.62 \pm 0.84
COVID-19 vs NO COVID-19	99.69 \pm 0.56	99.83 \pm 0.35	99.6 \pm 0.8	99 \pm 1.98	99.71 \pm 0.4	99.4 \pm 0.99
Multiclass	98.06 \pm 1.63	97.24 \pm 2.67	99.38 \pm 0.33	99.6 \pm 0.21	98.31 \pm 1.33	98.39 \pm 1.38

**Fig. 5.** Performance associated with the different kernel sizes for the three classification contexts under study. Scores evaluated were kappa and uncertainty.

the one between bacterial *vs* viral. This can be explained by the severity of the pulmonary affection that COVID-19 usually causes, whereas pneumonia derived from another viruses can show a more heterogeneous severity.

We observe that the discrimination ability of the system is very high for the three binary classifications regardless of the kernel size employed. Results in terms of different performance measures are shown in Table 1, whereas Figure 6 depicts the ROC curves for the different classifiers. Large values are obtained, as expected, in the CTL *vs* PNEU context. However, these results confirm that our system can also separate patients with the same diagnosis (pneumonia) but with a different cause (bacteria, virus, COVID-19). We also use the kappa-uncertainty diagram to evaluate the level of agreement between the classifier outputs. Figure 7 shows these diagrams for the three binary classifiers and the multiclass derived from the decision tree, represented by a different colour. The cloud points represent the kappa score-uncertainty obtained in each fold of the cross-validation scheme, whereas large stars represent the centroid of the resulting distribution. From this figure, we can see that there is not a great difference between individual classifiers, in consonance with results derived from ROC

curves.

It is interesting how this figure reveals that the combination of classifiers with a certain performance (high kappa score and low uncertainty) leads to an ensemble classifier with these features. However, uncertainty is higher in the multiclass classifier for a similar kappa score compared to individual ones. This means that, although classification performance of the decision tree is high, the uncertainty of the resulting prediction is also higher than in binary classification. This evidences the extreme utility of this kind of diagrams in Bayesian deep learning and in contexts when reliability of predictions is of core interest. According to Table 1, the multiclass classifier has a superior performance than the CTRL *vs* PNEU in most of metrics evaluated. However, the uncertainty of the predictions is also higher (centroid of the multiclass is farther to the right than the CTRL *vs* PNEU centroid). Further discussion regarding the results obtained and their clinical implications are provided in Section 6.

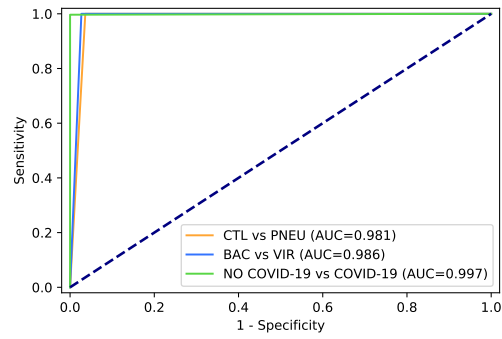


Fig. 6. ROC curves obtained by the classifiers of each level of the decision tree.

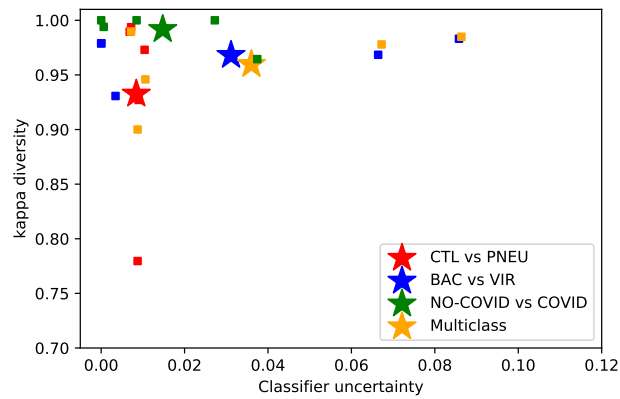


Fig. 7. Diversity-uncertainty diagrams of the different levels of the multiclass classifier. The x-axis represents the combined uncertainty of each individual classifier and the resulting multiclass. The y-axis represents diversity of the classifiers evaluated by the kappa measure. Each dot represents the kappa-uncertainty score obtained by a classifier in one fold, whereas large stars represent the centroid of the resulting distribution.

6. DISCUSSION

In this study, we proposed a classification method for the detection of different types of pneumonia from CXR images. This approach relies on the use of a Bayesian version of a Residual Network (ResNet), which allows the optimization of the network according to the uncertainty of its predictions. We employed different networks modifying their kernel sizes and combined them within an ensemble classifier so that the contribution of each individual network depends on the uncertainty of its predictions. We evaluated the performance of this approach in different classification scenarios. In the first context, the two classes generated relatively big differences in the observed pattern (pneumonia *vs* control), whereas in the second (bacterial *vs* viral pneumonia) and in the third one (COVID-19 *vs* no-COVID-19) these differences were extremely small. Besides, the performance of a multiclass classifier was also evaluated in order to check if this method could simultaneously differentiate between the different pathologies.

The high performance shown by the proposed method in all scenarios provides us with a new tool to detect the presence of pneumonia in CXR images, in addition to distinguish whether the source of the pathology is viral or bacterial, and if the virus is COVID-19 or not. The features extracted by convolutional blocks of different kernel sizes contained relevant information that enhanced the separability between the different classes. The combination of convolutional blocks of different kernel sizes is especially interesting in this context where the database contains images of people from a wide range of age. Pulmonary affections caused by the different pathologies evaluated in this work mainly depend on the severity of the disease. However, the shape and size of these manifestations also depend on the shape and size of lungs. The ensemble method proposed in this work allows the identification of patterns associated with pneumonia without focusing on a specific size for the informative regions.

Another crucial aspect of the method proposed in this work is its Bayesian nature. The aim of CAD systems regardless of the application context is to maximize the classification performance, in terms of accuracy, AUC, etc. However, in most scenarios it is also important to know the reliability of the prediction itself. Neural networks are prone to overfitting, which means that taking decisions based only on the prediction can be counterproductive. In an extreme case, it is possible that the classifier does not know the class a test image belongs to, but it always has to assign a label, even though the output probability is near to chance level. This is particularly problematic when developing a tool for the diagnosis of a disease. Doctors need to know not only the global accuracy obtained during the training and test of the model, but how reliable is the prediction of new individual samples. This problem is addressed with the inclusion of Bayesian elements in neural networks. However, our findings reveal that this is not the only advantage that this approach provides. We

have demonstrated the high performance of ensemble classification, even in situations where differences between the pulmonary patterns of the different pathologies are extremely small. The novelty of our approach relies on the way the contribution of each individual classifier to the global decision is computed. Weights are usually derived from the accuracy of each individual classifier. However, results can be biased if part of the predictions are obtained by chance, i.e. when the output probabilities of the different classes are almost equal. We overcome this problem by weighting the contribution of each classifier according to the uncertainty of its predictions.

It is worth remembering that part of the database (normal, bacterial and viral (no-COVID) pneumonia patients) contains pediatric chest radiographies, whereas COVID-19 images correspond to adults. Detecting pneumonia from pediatric chest radiographies is more challenging than in adults for several reasons. First, the dose of X-ray radiation is considerably lower than in adults, which results in a reduced image resolution and a higher overlapping between the different anatomical parts. Second, lungs appearance changes dramatically along the pediatric development stages, both in size and shape (more similar to a triangle in infants). The dataset employed in this work contains CXR images of children of a wide range of ages, increasing variability and complexity of the classification process. Finally, CXRs are noisier than in adults because of movement, legs positioning or when they are being hold by adult hands. For this reason, it is worth highlighting the high performance obtained in this work, improving the results obtained in previous works even when applied to detect pneumonia in children (Jain et al., 2020b; Liang and Zheng, 2020; Rajaraman et al., 2018), adults (Schwyzer et al., 2020; Toğaçar et al., 2020; Yu et al., 2021), and also when tried to identify the presence of COVID-19 (Jain et al., 2020a; Mahmud et al., 2020; Panwar et al., 2020; Wang et al., 2021b).

We have developed a tool that is able to distinguish between patterns associated with different pathologies, but it is worth highlighting the high performance obtained in the multiclass classification. In this case, the accuracy and the AUC obtained were 98.06% and 98.31%, respectively, which is considerably higher than the results provided by similar techniques in previous studies (Apostolopoulos and Tzani, 2020; Hemdan et al., 2020; Wang et al., 2020; Zhang et al., 2020; Zhou et al., 2020). There are two main relevant aspects derived from these excellent results to be mentioned. First, the only preprocessing applied to the data was the rescaling of the images to a lower resolution in order to reduce the computational burden of the classification pipeline. We did not perform other complex processes such as lung segmentation, but the RAW rescaled images were used as the inputs of the classification system. Thus, it is remarkable the high performance obtained by the method proposed in this extreme situation. Second, results obtained in the multiclass scenario allow the application of the tool proposed in this work in a

more real context. The multiclass scenario is more similar to a real context than binary classifications, where the simplest case only distinguishes the presence (or not) of pneumonia. Results obtained by the multiclass classifier reveal the usefulness of this kind of techniques.

7. CONCLUSION

Respiratory illness is leading cause of death and disability in the world. The annual fatality rate of pneumonia is approximately 4 million people, whereas is the leading cause of death among children under 5 years old. The pathology associated with pneumonia is often overlapping with other abnormal conditions of the lung, leading to a time-consuming process that may delay diagnosis and treatment. In this paper we proposed an uncertainty-driven ensemble of deep neural networks to identify patterns associated with different types of pneumonia. This tool combined the information extracted from different architectures according to the uncertainty of their predictions, instead of using the accuracy of individual classifiers as most studies usually do. The information provided about the reliability of the predictions, in addition to the large performance obtained (accuracy of 98.06% when distinguished between four pathologies) evidences the applicability of the system to be used as an aid for clinicians. The combination of CNNs of different kernel sizes allows the identification of pneumonia patterns regardless of their size and shape. Moreover, the reduced preprocessing needed for obtaining these results guarantees a limited computational cost. Our results pave the way for the application of Bayesian deep neural networks to other image modalities such as CT, which offers much more resolution than XR images and can provide key information for the detection of pneumonia.

Acknowledgments

This work was partly supported by the MINECO/ FEDER under the PGC2018-098813-B-C32, RTI2018-098913-B100, CV20-45250 and A-TIC-080-UGR18 projects.

References

- Abiyev, R., Ma'aitah, M., 08 2018. Deep convolutional neural networks for chest diseases detection. *Journal of Healthcare Engineering* 2018, 1–11.
- Ahmad, W. S. H. M. W., Zaki, W. M. D. W., Fauzi, M. F. A., 2015. Lung segmentation on standard and mobile chest radiographs using oriented gaussian derivatives filter. *BioMedical Engineering OnLine* 14.
- Ajin, M., Mredhula, L., 2017. Diagnosis of interstitial lung disease by pattern classification. *Procedia Computer Science* 115, 195 – 208, 7th International Conference on Advances in Computing & Communications, ICACC-2017, 22-24 August 2017, Cochin, India.
- Apostolopoulos, I., Tzani, M., 03 2020. Covid-19: Automatic detection from X-ray images utilizing transfer learning with convolutional neural networks. *Australasian physical & engineering sciences in medicine / supported by the Australasian College of Physical Scientists in Medicine and the Australasian Association of Physical Sciences in Medicine* 43.
- Candemir, S., Jaeger, S., Palaniappan, K., Musco, J. P., Singh, R. K., Xue, Z., Karargyris, A., Antani, S., Thoma, G., McDonald, C. J., 2014. Lung segmentation in chest radiographs using anatomical atlases with nonrigid registration. *IEEE Transactions on Medical Imaging* 33 (2), 577–590.
- Castillo-Barnes, D., Ramírez, J., Segovia, F., Martínez-Murcia, F. J., Salas-Gonzalez, D., Górriz, J. M., 2018. Robust ensemble classification methodology for i123-ioflupane SPECT images and multiple heterogeneous biomarkers in the diagnosis of Parkinson's disease. *Frontiers in Neuroinformatics* 12, 53.
- Chandra, T. B., Verma, K., Singh, B. K., Jain, D., Netam, S. S., 2020. Automatic detection of tuberculosis related abnormalities in chest X-ray images using hierarchical feature extraction scheme. *Expert Systems with Applications* 158, 113514.
- Chandra, T. B., Verma, K., Singh, B. K., Jain, D., Netam, S. S., 2021. Coronavirus disease (COVID-19) detection in chest X-ray images using majority voting based classifier ensemble. *Expert Systems with Applications* 165, 113909.
- Chapman, B. E., Lee, S., Kang, H. P., Chapman, W. W., 2011. Document-level classification of CT pulmonary angiography reports based on an extension of the context algorithm. *Journal of Biomedical Informatics* 44 (5), 728 – 737.
- Chen, C.-H., Huang, W.-T., Tan, T.-H., Chang, C.-C., Chang, Y.-J., 2015. Using k-nearest neighbor classification to diagnose abnormal lung sounds. *Sensors (Basel, Switzerland)* 15, 13132 – 13158.

- Cipolla, R., Gal, Y., Kendall, A., 2018. Multi-task learning using uncertainty to weigh losses for scene geometry and semantics. In: 2018 IEEE/CVF Conference on Computer Vision and Pattern Recognition. pp. 7482–7491.
- Cohen, J., 1960. A coefficient of agreement for nominal scales. *Educational and Psychological Measurement* 20, 37 – 46.
- Damianou, A., Lawrence, N., 2013. Deep gaussian processes. Vol. 31 of *Proceedings of Machine Learning Research*. PMLR, pp. 207–215.
- Di Eugenio, B., Glass, M., 2004. The kappa statistic: A second look. *Comput. Linguist.* 30 (1), 95–101.
- Elaziz, M. A., Hosny, K. M., Salah, A., Darwish, M. M., Lu, S., Sahlol, A. T., 2020. New machine learning method for image-based diagnosis of covid-19. *PLOS ONE* 15 (6), 1–18.
- Feng, F., Xia, G., Wang, Q., Shi, Y., Zhang, Z., 2015. Initial computed tomography findings of pneumonia in patients with human infected avian influenza (H7N9). *Radiology of Infectious Diseases* 1 (2), 57 – 63.
URL <http://www.sciencedirect.com/science/article/pii/S2352621115000066>
- Gal, Y., 2016. Uncertainty in deep learning. Ph.D. thesis, University of Cambridge.
- Galar, M., Fernández, A., Barrenechea, E., Bustince, H., Herrera, F., 2011. An overview of ensemble methods for binary classifiers in multi-class problems: Experimental study on one-vs-one and one-vs-all schemes. *Pattern Recognition* 44 (8), 1761 – 1776.
- Gao, X., He, Y., Zhang, M., Diao, X., Jing, X., Ren, B., Ji, W., 2021. A multiclass classification using one-versus-all approach with the differential partition sampling ensemble. *Engineering Applications of Artificial Intelligence* 97, 104034.
- Gilani, Z., Kwong, Y., Levine, O., Deloria-Knoll, M., Scott, J. A., O'Brien, K., Feikin, D., 04 2012. A literature review and survey of childhood pneumonia etiology studies: 2000–2010. *Clinical infectious diseases: an official publication of the Infectious Diseases Society of America* 54 Suppl 2, S102–8.
- Górriz, J., Ramírez, J., Ortíz, A., Martínez-Murcia, F., Segovia, F., Suckling, J., Leming, M., Zhang, Y., Álvarez Sánchez, J., Bologna, G., Bonomini, P., Casado, F., Charte, D., Charte, F., Contreras, R., Cuesta-Infante, A., Duro, R., Fernández-Caballero, A., Fernández, J., 2020. Artificial intelligence within the interplay between natural and artificial computation: Advances in data science, trends and applications. *Neurocomputing* 410, 237–270.
URL <http://dx.doi.org/10.1016/j.neucom.2020.05.078>
- Gu, X., Pan, L., Liang, H., Yang, R., 2018. Classification of bacterial and viral childhood pneumonia using deep learning in chest radiography. In: *Proceedings of the 3rd International Conference on Multimedia and Image Processing. ICMIP 2018*. Association for Computing Machinery, New York, NY, USA, p. 88–93.
URL <https://doi.org/10.1145/3195588.3195597>
- Guan, Q., Huang, Y., 2020. Multi-label chest X-ray image classification via category-wise residual attention learning. *Pattern Recognit. Lett.* 130, 259–266.
- Hajian-Tilaki, K., 09 2013. Receiver operating characteristic (ROC) curve analysis for medical diagnostic test evaluation. *Caspian journal of internal medicine* 4, 627–635.
- Hassen, D. B., Taleb, H., Yaakoub, I. B., Mnif, N., 2013. A Fuzzy Approach to Chest Radiography Segmentation Involving Spatial Relations. *International Journal of Computer Applications*.
- He, K., Zhang, X., Ren, S., Sun, J., 2016. Deep residual learning for image recognition. In: *2016 IEEE Conference on Computer Vision and Pattern Recognition (CVPR)*. pp. 770–778.
- Hemdan, E. E.-D., Shouman, M. A., Karar, M. E., 2020. COVIDX-Net: A framework of deep learning classifiers to diagnose COVID-19 in X-ray images.
- Hogeweg, L., Sánchez, C. I., Maduskar, P., Philipsen, R., Story, A., Dawson, R., Theron, G., Dheda, K., Peters-Bax, L., van Ginneken, B., 2015. Automatic detection of tuberculosis in chest radiographs using a combination of textural, focal, and shape abnormality analysis. *IEEE Transactions on Medical Imaging* 34 (12), 2429–2442.
- J, A., M, A., Daniel, A., Singerji, A., 2017. A robust automated lung segmentation system for chest X-ray (CXR) images. *International Journal of Engineering Research and* 6.
- Jaeger, S., Karargyris, A., Candemir, S., Folio, L., Siegelman, J., Callaghan, F., Xue, Z., Palaniappan, K., Singh, R. K., Antani, S., Thoma, G., Wang, Y., Lu, P., McDonald, C. J., 2014. Automatic tuberculosis screening using chest radiographs. *IEEE Transactions on Medical Imaging* 33 (2), 233–245.
- Jain, G., Mittal, D., Thakur, D., Mittal, M. K., 2020a. A deep learning approach to detect covid-19 coronavirus with X-ray images. *Biocybernetics and Biomedical Engineering* 40 (4), 1391 – 1405.

- Jain, R., Nagrath, P., Kataria, G., Sirish Kaushik, V., Jude Hemanth, D., 2020b. Pneumonia detection in chest X-ray images using convolutional neural networks and transfer learning. *Measurement* 165, 108046.
- Jospin, L. V., Buntine, W. L., Boussaid, F., Laga, H., Bennaoun, M., 2020. Hands-on bayesian neural networks - a tutorial for deep learning users. *ArXiv abs/2007.06823*.
- Kaggle, 2020a. Chest X-Ray Images (Covid-19 & Pneumonia). URL <https://www.kaggle.com/prashant268/chest-xray-covid19-pneumonia>
- Kaggle, 2020b. Chest X-Ray Images (Pneumonia) dataset. URL <https://www.kaggle.com/paultimothymooney/chest-xray-pneumonia?>
- Kendall, A., Gal, Y., 2017. What uncertainties do we need in bayesian deep learning for computer vision? In: Guyon, I., Luxburg, U. V., Bengio, S., Wallach, H., Fergus, R., Vishwanathan, S., Garnett, R. (Eds.), *Advances in Neural Information Processing Systems*. Vol. 30. Curran Associates, Inc., pp. 5574–5584.
- Kermany, D. S., Goldbaum, M., Cai, W., Valentim, C. C., Liang, H., Baxter, S. L., McKeown, A., Yang, G., Wu, X., Yan, F., Dong, J., Prasadha, M. K., Pei, J., Ting, M. Y., Zhu, J., Li, C., Hewett, S., Dong, J., Ziyar, I., Shi, A., Zhang, R., Zheng, L., Hou, R., Shi, W., Fu, X., Duan, Y., Huu, V. A., Wen, C., Zhang, E. D., Zhang, C. L., Li, O., Wang, X., Singer, M. A., Sun, X., Xu, J., Tafreshi, A., Lewis, M. A., Xia, H., Zhang, K., 2018. Identifying medical diagnoses and treatable diseases by image-based deep learning. *Cell* 172 (5), 1122 – 1131.e9.
- Kingma, D. P., Ba, J., 2017. Adam: A method for stochastic optimization.
- Kiureghian, A. D., Ditlevsen, O., 2009. Aleatory or epistemic? does it matter? *Structural Safety* 31 (2), 105 – 112, risk Acceptance and Risk Communication.
- Kohavi, R., 1995. A study of cross-validation and bootstrap for accuracy estimation and model selection. In: *Proceedings of the 14th International Joint Conference on Artificial Intelligence - Volume 2. IJCAI'95*. Morgan Kaufmann Publishers Inc., San Francisco, CA, USA, p. 1137–1143.
- Krizhevsky, A., Sutskever, I., Hinton, G., 01 2012. Image-net classification with deep convolutional neural networks. *Neural Information Processing Systems* 25.
- Kunz, W. G., Patzig, M., Crispin, A., Stahl, R., Reiser, M. F., Notohamiprodjo, M., 2018. The value of supine chest X-ray in the diagnosis of pneumonia in the basal lung zones. *Academic Radiology* 25 (10), 1252 – 1256.
- Le, Q. V., Smola, A. J., Canu, S., 2005. Heteroscedastic gaussian process regression. In: *Proceedings of the 22nd International Conference on Machine Learning. ICML '05*. Association for Computing Machinery, p. 489–496.
- Li, Y., Gal, Y., 2017. Dropout inference in bayesian neural networks with alpha-divergences. In: *ICML*.
- Liang, G., Zheng, L., 2020. A transfer learning method with deep residual network for pediatric pneumonia diagnosis. *Computer Methods and Programs in Biomedicine* 187, 104964.
- Liu, C., Pang, M., 2020. Automatic lung segmentation based on image decomposition and wavelet transform. *Biomedical Signal Processing and Control* 61, 102032.
- Liu, M., Zhang, D., Shen, D., 2012. Ensemble sparse classification of Alzheimer's disease. *NeuroImage* 60 (2), 1106 – 1116.
- Ma, L., Liu, X., Song, L., Zhou, C., Zhao, X., Zhao, Y., 2015. A new classifier fusion method based on historical and on-line classification reliability for recognizing common CT imaging signs of lung diseases. *Computerized Medical Imaging and Graphics* 40, 39 – 48.
- Maduskar, P., Philipsen, R., Melendez, J., Scholten, E., Chanda, D., Ayles, H., Sánchez, C., Ginneken, B., 12 2015. Automatic detection of pleural effusion in chest radiographs. *Medical Image Analysis* 28, 22–32.
- Mahmud, T., Rahman, M. A., Fattah, S. A., 2020. Covxnet: A multi-dilation convolutional neural network for automatic COVID-19 and other pneumonia detection from chest X-ray images with transferable multi-receptive feature optimization. *Computers in Biology and Medicine* 122, 103869. URL <http://www.sciencedirect.com/science/article/pii/S0010482520302250>
- Mandrekar, J. N., 2010. Receiver operating characteristic curve in diagnostic test assessment. *Journal of Thoracic Oncology* 5 (9), 1315 – 1316.
- Martínez-Murcia, F., Gorriz, J., Ramírez, J., Ortiz, A., 07 2018. Convolutional neural networks for neuroimaging in Parkinson's disease: Is preprocessing needed? *International Journal of Neural Systems* 28.
- Mittal, A., Kumar, D., Mittal, M., Saba, T., Abunadi, I., Rehman, A., s. Roy., 2020. Detecting pneumonia using convolutions and dynamic capsule routing for chest X-ray image. *Sensors* 20 (4), 1068.
- Nix, D. A., Weigend, A. S., 1994. Estimating the mean and variance of the target probability distribution. In: *Proceedings of 1994 IEEE International Conference on Neural Networks (ICNN'94)*. Vol. 1. pp. 55–60 vol.1.

- Ortiz, A., Martínez-Murcia, F., García-Tarifa, M., Lozano, F., Gorriz, J., Ramírez, J., 06 2016. Automated diagnosis of Parkinsonian syndromes by deep sparse filtering-based features. In: *Innovation in Medicine and Healthcare 2016*. pp. 249–258.
- Panwar, H., Gupta, P., Siddiqui, M. K., Morales-Menendez, R., Bhardwaj, P., Singh, V., 2020. A deep learning and grad-cam based color visualization approach for fast detection of COVID-19 cases using chest X-ray and CT-scan images. *Chaos, Solitons & Fractals* 140, 110190.
URL <http://www.sciencedirect.com/science/article/pii/S0960077920305865>
- Payan, A., Montana, G., 02 2015. Predicting Alzheimer's disease: a neuroimaging study with 3d convolutional neural networks. *ICPRAM 2015 - 4th International Conference on Pattern Recognition Applications and Methods, Proceedings 2*.
- Porcel, J. M., Alemán, C., Bielsa, S., Sarrapio, J., Fernández de Sevilla, T., Esquerda, A., 2008. A decision tree for differentiating tuberculous from malignant pleural effusions. *Respiratory Medicine* 102 (8), 1159 – 1164.
- Rajaraman, S., Candemir, S., Kim, I., Thoma, G., Antani, S., 09 2018. Visualization and interpretation of convolutional neural network predictions in detecting pneumonia in pediatric chest radiographs. *Applied Sciences* 8, 1715.
- Rajpurkar, P., Irvin, J., Zhu, K., Yang, B., Mehta, H., Du-an, T., Ding, D., Bagul, A., Langlotz, C., Shpanskaya, K., Lungren, M., Ng, A., 11 2017. Chexnet: Radiologist-level pneumonia detection on chest X-rays with deep learning.
- Rodriguez, J. J., Kuncheva, L. I., Alonso, C. J., 2006. Rotation forest: A new classifier ensemble method. *IEEE Transactions on Pattern Analysis and Machine Intelligence* 28 (10), 1619–1630.
- Schmidhuber, J., 2015. Deep learning in neural networks: An overview. *Neural Networks* 61, 85 – 117.
URL <http://www.sciencedirect.com/science/article/pii/S0893608014002135>
- Schwyzler, M., Martini, K., Skawran, S., Messerli, M., Frauenfelder, T., 2020. Pneumonia detection in chest X-ray dose-equivalent ct: Impact of dose reduction on detectability by artificial intelligence. *Academic Radiology*.
- Segovia, F., García-Pérez, M., Gorriz, J., Ramírez, J., Martínez-Murcia, F., 10 2016. Assisting the diagnosis of neurodegenerative disorders using principal component analysis and tensorflow. In: *International Joint Conference SOCO'16-CISIS'16-ICEUTE'16*. pp. 43–52.
- Srivastava, N., Hinton, G. E., Krizhevsky, A., Sutskever, I., Salakhutdinov, R., 2014. Dropout: a simple way to prevent neural networks from overfitting. *J. Mach. Learn. Res.* 15, 1929–1958.
- Syrjala, H., Broas, M., Ohtonen, P., Jartti, A., Pääkkö, E., 2017. Chest magnetic resonance imaging for pneumonia diagnosis in outpatients with lower respiratory tract infection. *European Respiratory Journal* 49 (1).
- Toğaçar, M., Ergen, B., Cömert, Z., Özyurt, F., 2020. A deep feature learning model for pneumonia detection applying a combination of mRMR feature selection and machine learning models. *IRBM* 41 (4), 212 – 222.
- Uppaluri, R., Hoffman, E., Sonka, M., Hartley, P., Hunninghake, G., McLennan, G., 1999. Computer recognition of regional lung disease patterns. *American journal of respiratory and critical care medicine* 160 (2), 648—654.
- Vajda, S., Karargyris, A., Jäger, S., Santosh, K. C., Candemir, S., Xue, Z., Antani, S. K., Thoma, G. R., 2018. Feature selection for automatic tuberculosis screening in frontal chest radiographs. *Journal of Medical Systems* 42, 1–11.
- Van Ginneken, B., Ter Haar Romeny, B. M., Viergever, M. A., 2001. Computer-aided diagnosis in chest radiography: a survey. *IEEE Transactions on Medical Imaging* 20 (12), 1228–1241.
- Varshni, D., Thakral, K., Agarwal, L., Nijhawan, R., Mittal, A., 2019. Pneumonia detection using CNN based feature extraction. In: *2019 IEEE International Conference on Electrical, Computer and Communication Technologies (ICECCT)*. pp. 1–7.
- Wang, H., Yeung, D., 2016. Towards bayesian deep learning: A framework and some existing methods. *IEEE Transactions on Knowledge and Data Engineering* 28, 3395–3408.
- Wang, J., Yang, Y., Xia, B., 2019. A simplified cohen's kappa for use in binary classification data annotation tasks. *IEEE Access* 7, 164386–164397.
- Wang, S., Kang, B., Ma, J., Zeng, X., Xiao, M., Guo, J., Cai, M., Yang, J., Li, Y., Meng, X., Xu, B., 2020. A deep learning algorithm using CT images to screen for corona virus disease (covid-19). *medRxiv*.
- Wang, S.-H., Govindaraj, V. V., Górriz, J. M., Zhang, X., Zhang, Y.-D., 2021a. Covid-19 classification by FGCNet with deep feature fusion from graph convolutional network and convolutional neural network. *Information Fusion* 67, 208 – 229.
URL <http://www.sciencedirect.com/science/article/pii/S1566253520303705>
- Wang, X., Peng, Y., Lu, L., Lu, Z., Bagheri, M., Summers, R. M., 2017. ChestX-Ray8: Hospital-Scale Chest X-Ray

- Database and Benchmarks on Weakly-Supervised Classification and Localization of Common Thorax Diseases. In: 2017 IEEE Conference on Computer Vision and Pattern Recognition (CVPR). pp. 3462–3471.
- Wang, Z., Xiao, Y., Li, Y., Zhang, J., Lu, F., Hou, M., Liu, X., 2021b. Automatically discriminating and localizing covid-19 from community-acquired pneumonia on chest X-rays. *Pattern Recognition* 110, 107613.
- White, G., 09 2008. Basics of estimating measurement uncertainty. *The Clinical biochemist. Reviews / Australian Association of Clinical Biochemists* 29 Suppl 1, S53–60.
- World Health Organization, 2016. Global tuberculosis report 2016.
URL http://www.who.int/tb/publications/global_report/en/
- World Health Organization, 2017. The global impact of respiratory diseases - second edition. Forum of International Respiratory Societies (FIRS).
- Xu, Y., van Beek, E. J., Hwanjo, Y., Guo, J., McLennan, G., Hoffman, E. A., 2006. Computer-aided classification of interstitial lung diseases via mdct: 3d adaptive multiple feature method (3d amfm). *Academic Radiology* 13 (8), 969 – 978.
- Yahyaoui, A., Yumusak, N., 2018. Decision support system based on the support vector machines and the adaptive support vector machines algorithm for solving chest disease diagnosis problems. *Biomedical Research-tokyo* 29, 1474–1480.
- Yang, W., Liu, Y., Lin, L., Yun, Z., Lu, Z., Feng, Q., Chen, W., 2018. Lung field segmentation in chest radiographs from boundary maps by a structured edge detector. *IEEE Journal of Biomedical and Health Informatics* 22 (3), 842–851.
- Yu, X., Wang, S.-H., Zhang, Y.-D., 2021. Cgnet: A graph-knowledge embedded convolutional neural network for detection of pneumonia. *Information Processing & Management* 58 (1), 102411.
- Zhang, K., Liu, X., Shen, J., Li, Z., Sang, Y., Wu, X., Zha, Y., Liang, W., Wang, C., Wang, K., Ye, L., Gao, M., Zhou, Z., Li, L., Wang, J., Yang, Z., Cai, H., Xu, J., Yang, L., Cai, W., Xu, W., Wu, S., Zhang, W., Jiang, S., Zheng, L., Zhang, X., Wang, L., Lu, L., Li, J., Yin, H., Wang, W., Li, O., Zhang, C., Liang, L., Wu, T., Deng, R., Wei, K., Zhou, Y., Chen, T., Lau, J. Y.-N., Fok, M., He, J., Lin, T., Li, W., Wang, G., 2020a. clinically applicable ai system for accurate diagnosis, quantitative measurements, and prognosis of covid-19 pneumonia using computed tomography”. *Cell* 181 (6), 1423 – 1433.e11.
- Zhang, Y.-D., Dong, Z., Wang, S.-H., Yu, X., Yao, X., Zhou, Q., Hu, H., Li, M., Jiménez-Mesa, C., Ramirez, J., Martinez, F. J., Gorriz, J. M., 2020b. Advances in multimodal data fusion in neuroimaging: Overview, challenges, and novel orientation. *Information Fusion* 64, 149 – 187.
- Zhang, Y. D., Satapathy, S. C., Zhu, L. Y., Górriz, J. M., Wang, S. H., 2020. A seven-layer convolutional neural network for chest CT based covid-19 diagnosis using stochastic pooling. *IEEE Sensors Journal*, 1–1.
- Zhou, L., Fujita, H., 2017. Posterior probability based ensemble strategy using optimizing decision directed acyclic graph for multi-class classification. *Information Sciences* 400-401, 142 – 156.
URL <http://www.sciencedirect.com/science/article/pii/S0020025516314207>
- Zhou, T., ling Lu, H., Yang, Z., Qiu, S., qiang Huo, B., Dong, Y., 2020. The ensemble deep learning model for novel covid-19 on CT images. *Applied Soft Computing*, 106885.